Graphitization during high-grade metamorphism in the southern Bohemian Massif

Gerd Rantitsch [a,*], Manfred Linner [b]

[a] *Department of Applied Geosciences and Geophysics, Montanuniversität Leoben, Peter-Tunner-Strasse 5, 8700 Leoben, Austria*
[b] *Geological Survey of Austria, Neulinggasse 38, 1030 Wien, Austria*

ARTICLE INFO

ABSTRACT

Raman spectroscopy on carbonaceous matter reconstructs the progressive path of graphitization during granulite facies metamorphism in the Variscan collisional belt of the southern Bohemian Massif. In this area, heating to 650–750 °C gradually altered the graphite microstructure, attributed to a metamorphic field gradient. Late low-pressure and high-temperature metamorphism at temperatures above 800 °C as well as advective heat transport due to rising granulite diapirs improved the graphite lattice ordering significantly. Numerical parameters derived from the Raman spectra of carbonaceous matter, in particular the G-band width and the S2-band dispersion map metamorphic field gradients in high-grade metamorphic terrains.

1. Introduction

Graphite, as the final product of organic metamorphism, occurs commonly in medium- to high-grade metamorphosed sediments (e.g. Landis, 1971). As graphitization proceeds over a wide range of metamorphic grade (Grew, 1974; Pasteris and Wopenka, 1991; Wopenka and Pasteris, 1993; Yui et al., 1996; Beyssac et al., 2002; Rantitsch et al., 2016a), precursor phases (anthracite, meta-anthracite, semi-graphite; Kwiecińska and Petersen, 2004) may be present together with graphite in the same sample (e.g. Kribek et al., 1994; Zheng et al., 1996). They can be classified by x-ray diffractometry, transmission electron microscopy and Raman spectroscopy to estimate the lattice dimensions and lattice ordering. Graphite occurs in the amphibolite facies and predominates the carbonaceous matter composition in the granulite facies of metamorphism (e.g. Rantitsch et al., 2016a). As demonstrated by empirical and experimental data (Bustin et al., 1995; Lyu et al., 2020; Nakamura et al., 2020), not only temperature, but also strain, time, and lithostatic pressure are important factors for the transformation of disordered carbonaceous matter to full-ordered graphite, commencing at 450 °C.

Interactive fitting of Raman spectra (IFORS; Lünsdorf et al., 2017) collected on carbonaceous matter was demonstrated as an effective tool to map the three-dimensional metamorphic pattern of low- to medium-grade metamorphic domains (Rantitsch et al., 2020; Groß et al., 2020). However, the calibration range of this method is limited to temperatures

of 160 °C to 600 °C. Although, this range covers the major segments of an orogen, the IFORS method cannot be used in its high-grade metamorphic terrains. As disseminated carbonaceous matter is omnipresent in crustal rocks, and is also concentrated locally in its deepest layer (e.g. Schrauder et al., 1993; Zhang et al., 2014; Cui et al., 2017; Miranda et al., 2019; Gautneb et al., 2020), an extension of the IFORS methods for high-grade metamorphic rocks may be of particular interest, as more elaborate thermometric techniques often do not allow mapping P-T conditions in a high sample density.

The aim of this study is to test the IFORS method in amphibolite- and granulite-facies metamorphic sediments of the southern Bohemian Massif (Fig. 1). In the study area, the Moldanubian Zone evolved from the Carboniferous continental collision during the Variscan orogeny, connected with the subduction of light felsic material and crustal overturns (Schulmann et al., 2005) with granulites in diapir-shaped crustal structures (Franĕk et al., 2006). Therefore, the Variscan orogen shows here characteristics of a "large hot orogen" (Jamieson and Beaumont, 2013). In the Moldanubian Zone, (formerly mined) graphite occurrences are known from numerous occurrences (Schrauder et al., 1993) with well-constrained P-T-t conditions of the host rocks (Petrakakis, 1997; Sorger, 2020; Sorger et al., 2020). Graphitic gneisses are also present both in the tectonic footwall and hangingwall of the graphite seams with P-T peak conditions between 0.75 and 1.1 GPa and 630–800 °C (Petrakakis, 1997; Racek et al., 2006; Sorger et al., 2020), thus covering the main zone of graphitization (Rantitsch et al., 2016a).
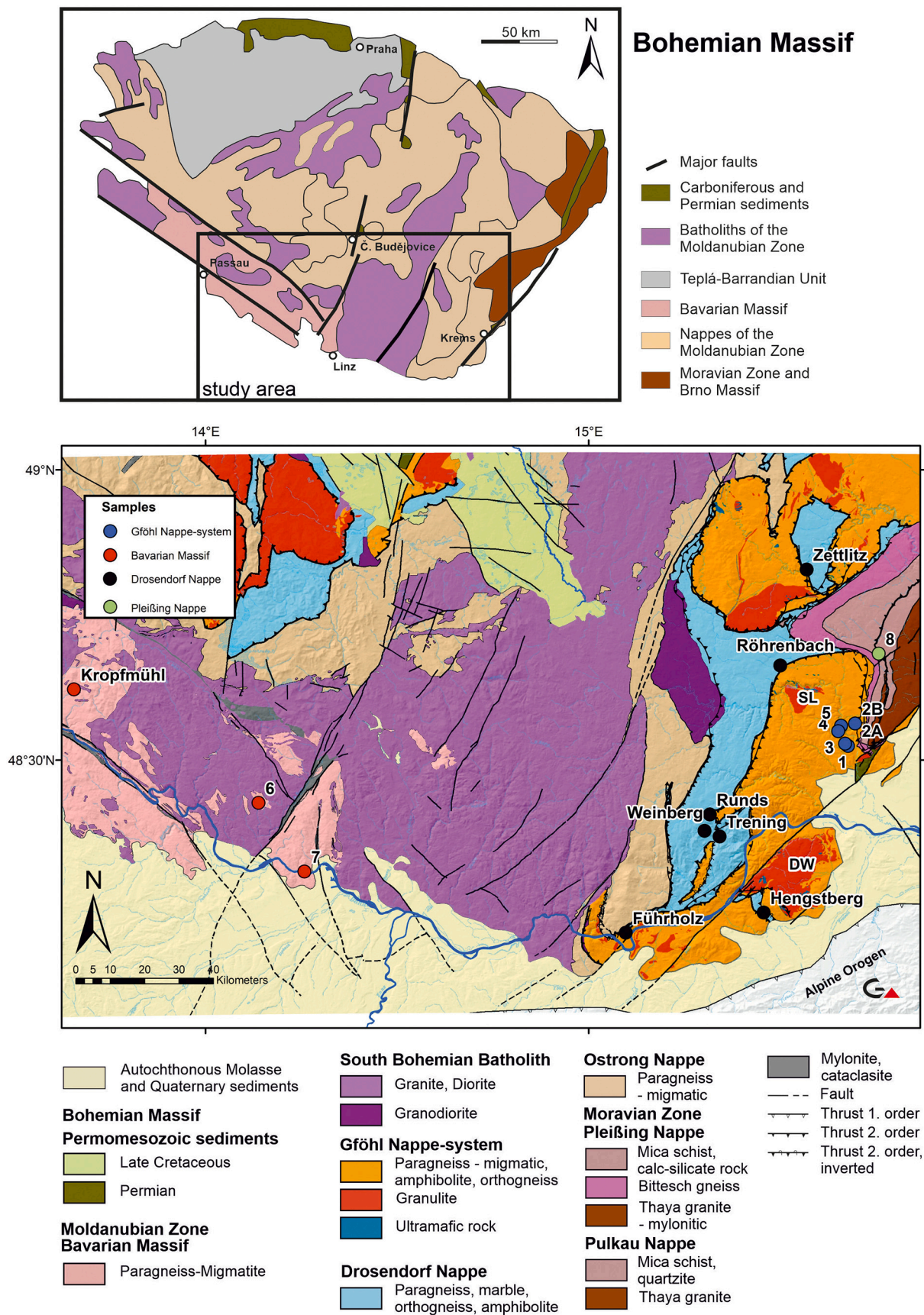

Fig. 1. Study area with the sample localities (names indicate sampled graphite mines) within the Bohemian Massif. DW = granulite diapir of Dunkelsteinerwald, SL = granulite diapir of Sankt Leonhard.

Table 1

Investigated samples (locality names indicate graphite mines) from the Bohemian Massif (coordinates are given in the EPSG 32633 reference system). In some samples large flake graphite crystals occur.

Sample		UTM33-N	UTM33-E	Tectonic unit	Lithology
1		5,374,837	549,978	Gföhl Nappe-system	Graphite quartzite
2A		5,379,147	551,306		Graphitic paragneiss
2B		5,379,147	551,306		Graphite quartzite
3		5,375,248	549,404		
4	Flake graphite	5,377,654	548,069		
5	Flake graphite	5,378,697	548,617		
6	Flake graphite	5,364,000	436,255	Bavarian massif	Graphitic paragneiss
7	Flake graphite	5,350,658	444,976		
Kropfmühl	Flake graphite	5,386,336	400,994		Graphite concentrate
Führholz	Flake graphite	5,338,565	507,217	Drosendorf Nappe	Graphite schist
Hengstberg	Flake graphite	5,342,579	533,910		
Zettlitz		5,408,568	541,764		
Runds		5,361,451	523,408		
Weinberg		5,358,303	522,415		
Röhrenbach		5,390,178	536,840		
Trening		5,357,211	525,326		
8		5,392,600	555,730	Pleißing Nappe	Graphite micaschist

As segments of the Moldanubian Zone, like the Bavarian Massif, were overprinted by low-pressure and high-temperature metamorphism at temperatures above 830 °C (Sorger et al., 2018), also the far advanced transformation of graphite during regional metamorphism is recorded in the investigated sample-set.

2. Geological setting

The southeastern margin of the Bohemian Massif (Fig. 1) exposes the Moldanubian and Moravian Zone assembled by Variscan (Late Devonian to Carboniferous) tectonics (e.g. Fritz et al., 1996; Schulmann et al., 2005). From the footwall to the top, the Ostrong Nappe, Drosendorf Nappe, and Gföhl Nappe-system comprise the Moldanubian Zone (Cháb et al., 2010; Linner et al., 2013). The representative age of 340 Ma for peak metamorphism of granulites (e.g. Schulmann et al., 2005; Friedl et al., 2011) sets the upper limit for exhumation. Thrusting of the resultant overturned thickened crust of the Moldanubian Zone on the Moravian Zone took place between 340 and 337 Ma (Štípská et al., 2015), followed by post-metamorphic cooling through 400 °C at ca. 330 Ma (Dallmeyer et al., 1992). The South Bohemian batholith intruded the overturned crust between 330 and 310 Ma (Klötzli et al., 1999; Finger et al., 2009).

In the Moravian Zone an upright rising metamorphic temperature gradient is constrained by peak metamorphism up to amphibolite-facies conditions (Štípská et al., 2015). In contrary, an overall inverse temperature gradient is characteristic for the Moldanubian Zone with granulite-facies metamorphic conditions in the Ostrong Nappe (Linner, 1996), Drosendorf Nappe (Petrakakis, 1997; Racek et al., 2006; Sorger, 2020; Sorger et al., 2020) and Gföhl Nappe-system (Petrakakis, 1997). Granulites within the Gföhl Nappe-system were metamorphosed during the Variscan collision at high-pressure and ultra-high-temperature peak conditions (Cooke and O'Brien, 2001; Schantl et al., 2019) and rapidly exhumed in folded and overturned sections of the orogenic middle crust (Franěk et al., 2006; Petri et al., 2014). In the Bavarian Massif at the southwestern margin of the Bohemian Massif, parts of the Moldanubian Zone were overprinted by a high-temperature and low-pressure event (Finger et al., 2007; Sorger et al., 2018) due to delamination of the lithospheric mantle in the late stage of the Variscan orogeny (Finger et al., 2009).

3. Samples

Seven graphite schist samples from the Drosendorf Nappe of the Moldanubian Zone come from closed graphite mines (Schrauder et al., 1993). Six samples from the Gföhl Nappe-system are metasediments with disseminated graphite. Two metasediment samples as well as a
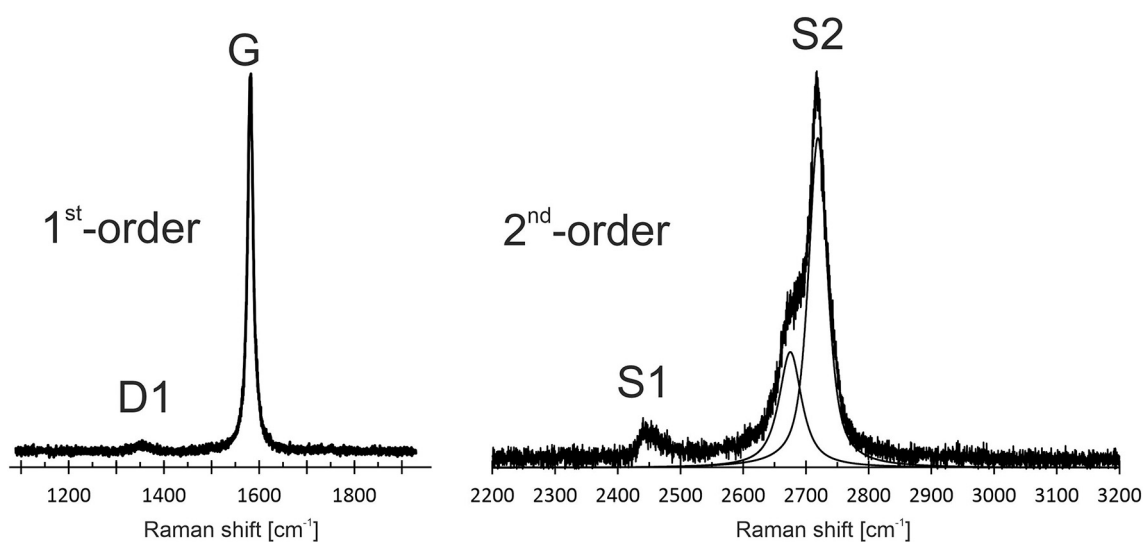

Fig. 2. Representative 1st- and 2nd-order Raman spectra of graphite (Hengstberg sample) showing a sharp G-band, a D1-band of very low intensity and asymmetric S1 and S2-bands. A D2-band at the right shoulder of the G-band is missing. The S2-band is deconvoluted into two Pseudo-Voigt functions.
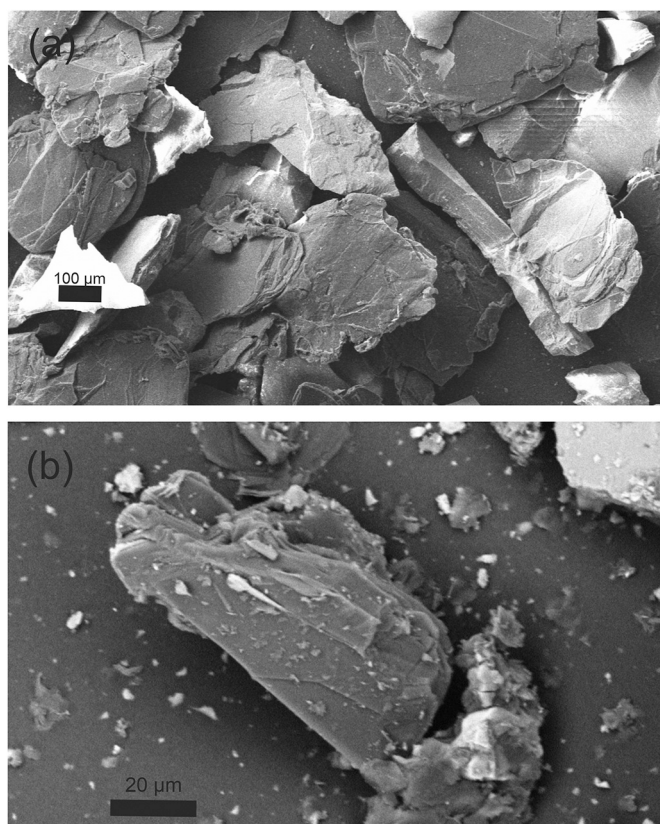
Fig. 3. Representative SEM images of graphite from the samples 7 (a) and Zettlitz (b). Note the large ca. 40 μm thick flakes in (a). The graphite crystal in (b) represents the predominant crystal size in the Zettlitz sample.
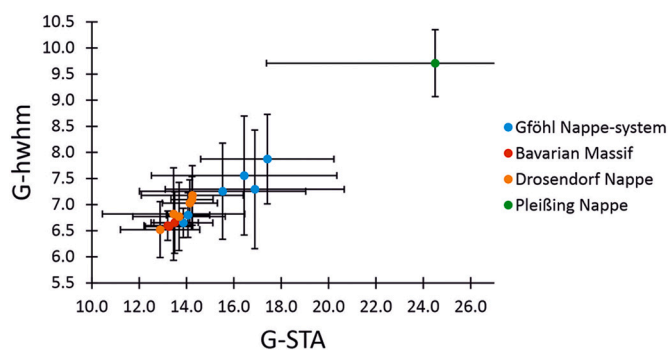

Fig. 4. G (graphite) band width (G-hwhm) versus G-STA (Lünsdorf et al., 2017). Decreasing G-hwhm and G-STA values (error bars indicate the standard deviation) indicate a better structural order.

graphite concentrate of the Kropfmühl mine derive from the Bavarian Massif. One sample from the Pleißing Nappe in the Moravian Zone completes the dataset (Fig. 1, Table 1). To compare the Raman spectra with spectra from samples metamorphosed at lower temperatures, four reference samples from previous studies (Lünsdorf et al., 2017; Iglseder et al., 2019; Rantitsch et al., 2020, Table 2) are used as well. The P-T-t-path of the investigated samples are constrained by precise thermo-chronological data as follows:

The metasedimentary host rock sequence of the Drosendorf Nappe ("Variegated complex") exposed at the Zettlitz graphite mine shows a P-T maximum of 0.8 GPa and ca. 700 °C (Racek et al., 2006), and ca. 0.6 GPa at 672 °C according to Sorger (2020). A higher P-T maximum of 0.95–1.10 GPa and 745–785 °C at 343 Ma was estimated by Sorger et al. (2020) in paragneisses at the southern segment of the same sequence. During 340–335 Ma granulites were exhumed rapidly (Petri et al., 2014; Schantl et al., 2019) in diapir-shaped structures from a P-T maximum of 1.6 GPa and 1000 °C (Schantl et al., 2019). In modern map view, they are part of the Gföhl Nappe-system (Linner et al., 2013), characterized by a metamorphic overprint at 700–800 °C and 0.8–1.1 GPa (Petrakakis, 1997). In the Bavarian Massif, low-pressure-high-temperature metamorphism with 830–900 °C at 0.55–0.65 GPa at 312 Ma (Sorger et al., 2018, see also Tropper et al., 2006 and Wyhlidal et al., 2009) overprinted parts of the Moldanubian nappe-systems. P-T conditions of the Pleißing Nappe sample are given by 0.6–0.7 GPa and 600–640 °C at 340–337 Ma (Štípská et al., 2015).

4. Analytical methods

Graphite from the graphite schist and the graphite ore sample were investigated without any sample treatment. Carbonaceous matter from the other samples was concentrated by an acid treatment of sample powder (crushed in an agate mortar mill for max. 20 s and sieved to <125 μm): The sample was placed into concentrated HCl, heated moderately for ca. 8 h and subsequently washed by distilled water. The dried residue was placed into concentrated HF, heated moderately for ca. 8 h, subsequently washed by distilled water and dried. Concentrates and untreated samples were mounted as a water-suspension on a glass slide. After drying, all samples were analyzed without polishing. A ZEISS® EVO MA 10 SEM equipped with a tungsten filament was used to image representative graphite concentrates at 15 kV on Au-coated specimens.

A Horiba Labram HR Evolution instrument, equipped with a 100 mW Nd:Yag (532 nm) laser, a confocal microscope (hole aperture = 100 μm), a 1800 g/mm grating, and a Peltier cooled CCD detector was used to collect Raman spectra. Two scans were averaged. 20 spectra over the 700–2000 cm^{-1} (first order) region and 16–20 spectra over the 2200–3200 cm^{-1} (second order) region (see Pimenta et al., 2007) were recorded on visible graphite basal planes for each sample. The wavenumbers were calibrated with the Rayleigh scattering (0 cm^{-1}), and a silicon wafer (520.7 cm^{-1}).

The band nomenclature follows the commonly applied terminology as reviewed by Henry et al. (2019), discriminating the G- ("graphite" band at ca. 1580 cm^{-1}), D1- (disorder band at ca. 1340 cm^{-1}) and D2- (disorder band at ca. 1610 cm^{-1}) bands in the first-order region as well as the S1- and S2 (at ca. 2700 cm^{-1}) bands in the second-order region (Fig. 2). The first-order Raman spectra were evaluated by the IFORS software of Lünsdorf and Lünsdorf (2016), excluding subjectivity in curve-fitting (Lünsdorf et al., 2014) by fitting the spectra without user-interaction. The spectra were characterized by spectral parameters (G-STA= total area, scaled by the G maximum intensity, G-shape factor, Gmax-position= band position of the G-band maximum) of Lünsdorf et al. (2017) estimated by the median of all collected first-order spectra. To estimate the G-band widths (G-hwhm = G-band half-width at half-maximum), the minimum distance between adjacent functions was adjusted to 300 in order to represent the band by a single function. The S2-band of the second-order spectrum was deconvoluted into two Pseudo-Voigt functions (Fig. 2) after removing a linear background by using the Fityk 1.3.1 software (Wojdyr, 2010).

Table 2

Raman spectral parameter estimated on graphite basal plains from the Bohemian Massif, completed by data from CM used for the IFORS-thermometry at temperatures below ≤600 °C (G-STA = scaled total area, scaled by the G maximum intensity, G-shape factor of Lünsdorf et al., 2017, Gmax position = band position of the G-band maximum, std. = standard deviation). G-hwhm = G-band half-width at half-maximum. D-band dispersion = number of S2 spectra with a deconvoluted Raman shift distance in the given interval. Reference temperatures (Temp = metamorphic temperature in °C estimated petrologically) from the cited studies are given for six graphite samples and for four IFORS calibration samples.

Sample	N	G_STA		G-shape factor		Gmax position		G-hwhm		D-band dispersion				Temp (°C)	Reference
		median	std	median	std	median	std	median	std	<35 cm^{-1}	35-39 cm^{-1}	39-44 cm^{-1}	>44 cm^{-1}		
1	20	16.9	3.8	14.8	4.9	1579.3	2.4	7.3	1.1	1	10	9	0		
2A	20	17.4	2.8	14.7	4.3	1580.6	1.9	7.9	0.9	0	6	13	1		
2B	20	15.5	3.5	18.7	5.1	1579.6	1.8	7.3	0.9	2	4	10	2		
3	20	16.4	3.9	14.5	5.3	1578.1	3.8	7.6	1.1	1	7	9	0		
4	20	13.9	1.2	21.8	2.9	1580.8	1.2	6.7	0.3	0	1	7	12		
5	20	14.1	0.9	19.2	2.1	1581.5	0.9	6.8	0.4	0	4	8	8		
6	20	13.5	1.3	20.3	2.4	1581.7	1.1	6.7	0.5	0	4	3	9	860	Sorger et al. (2018)
7	20	13.2	1.8	21.4	3.3	1581.5	0.9	6.6	0.6	0	1	10	9	860	Sorger et al. (2018)
Kropfmühl	20	13.3	0.8	21.6	1.2	1581.7	0.7	6.6	0.3	0	1	4	13		
Führholz	20	13.7	0.9	20.4	1.9	1581.7	1.6	6.8	0.4	0	2	12	6	790	Sorger et al. (2020)
Hengstberg	20	12.9	0.7	21.9	1.2	1581.3	1.0	6.5	0.2	0	1	3	13		
Zettlitz	20	14.3	2.1	19.3	3.1	1581.2	0.9	7.2	0.6	0	7	12	0	672	Sorger et al. (2020)
Runds	20	14.2	2.0	19.8	2.7	1580.5	1.2	7.2	0.7	19	1	0	0		
Weinberg	20	14.2	1.2	20.1	3.3	1580.0	3.1	7.1	0.4	1	9	10	0		
Röhrenbach	20	14.1	3.0	20.1	3.4	1579.8	1.7	7.0	0.9	0	5	14	0	715	Sorger et al. (2020)
Trening	20	13.5	1.7	21.3	3.5	1580.8	2.6	6.8	0.5	2	10	8	0		
8	20	15.5	2.8	18.4	3.7	1581.2	1.6	7.4	0.6	0	1	18	1	620	Štípská et al. (2015)
	20	24.5	7.1	9.3	3.6	1577.8	3.5	9.7	1.6	3	7	3	0		
IFORS calibration data															
KL16–27	30	16.2	1.0	53.0	4.8	4.1	0.5	1575.5	2.8					440	Lünsdorf et al. (2017)
KL14–52	21	11.9	3.2	34.1	6.0	5.8	1.7	1572.5	3.1					520	Lünsdorf et al. (2017)
IGL16–03	28	12.0	1.2	30.8	5.7	7.5	1.8	1577.9	2.9					535	Rantitsch et al. (2020)
IGL14–33	28	10.2	1.3	25.6	3.6	7.8	1.7	1577.7	3.3					600	Iglseder et al. (2019)

5. Results

Flake graphite samples with 200–400 μm large and 40–60 μm thick crystals are discriminated from samples with significantly smaller (<100 μm) graphite crystals (Fig. 3b). Large flakes are found in two samples of the Drosendorf Nappe, in two samples of the Gföhl Nappe-system, and in the Bavarian Massif samples (Table 1).

The Raman spectra are characterized by an intense G-band and low-intensity or even missing D1- and D2-bands (Fig. 2). The dominant second order S2-band (Fig. 2) splits into two bands (see Cançado et al., 2008; Rantitsch et al., 2016a; Skrzypek, 2021), indicating a triperiodic graphite structure (Pimenta et al., 2007; Cançado et al., 2008; Rantitsch et al., 2016a), commonly occurring at metamorphic temperatures above 500 °C (Skrzypek, 2021). The G-band width and the spectral parameters (G-STA and G-shape factor of Lünsdorf et al., 2017, Gmax position) are correlated (Fig. 4, Table 2).

Lower G-STA values are related to lower G-hwhm values (Fig. 4) and correlated to higher G-shape factors (Table 2). As decreasing G-STA values indicate higher metamorphic temperatures between 400 and 600 °C (Lünsdorf et al., 2017), a trend to lower G-STA (Lünsdorf et al., 2017) and G-hwhm (Rantitsch et al., 2016a, 2016b) values indicates a better microstructural order of the graphite lattice. Accordingly, the highest graphite order (G-STA < 14.1 and G-hwhm <7) is observed in the flake graphite sample group (Table 2), characterized also by very low or missing D1- and D2-bands (see Fig. 2 for an example). Graphite from sample 8 (Pleißing Nappe) occurs in two crystal size classes. Crystals smaller than 4 μm show a lower structural order than the larger class (Table 2). The Raman parameters of the tiny crystals are in accordance to the reported metamorphic conditions (Table 2) and therefore used to describe the graphitization rank of this sample.

The distance between the two function maxima of the deconvoluted S2-band (Fig. 2) varies between 28 and 46 cm^{-1} (Fig. 5a), with a significant within-sample variation (Table 2, Fig. 5b). Breaks in a probability plot at 35, 39, and 44 cm^{-1} demonstrate the presence of several data populations among all samples (Fig. 5a). Based on this plot, four individual structural groups are discriminated (natural break classification). As a singular sample is typically characterized by three S2 dispersion groups (Fig. 5b, Table 2), the structural state of a sample is not represented by any sample mean of the S2-band distances. Therefore, the S2-band of a sample is characterized here by the proportion of the S2 dispersion group memberships, constrained by samples of known metamorphic conditions (Fig. 5b, Table 2). The results indicate a continuous structural evolution of an increasing S2 dispersion with rising metamorphic conditions, bracketed by a temperature uncertainty of ca. ±30 °C (Fig. 5b).
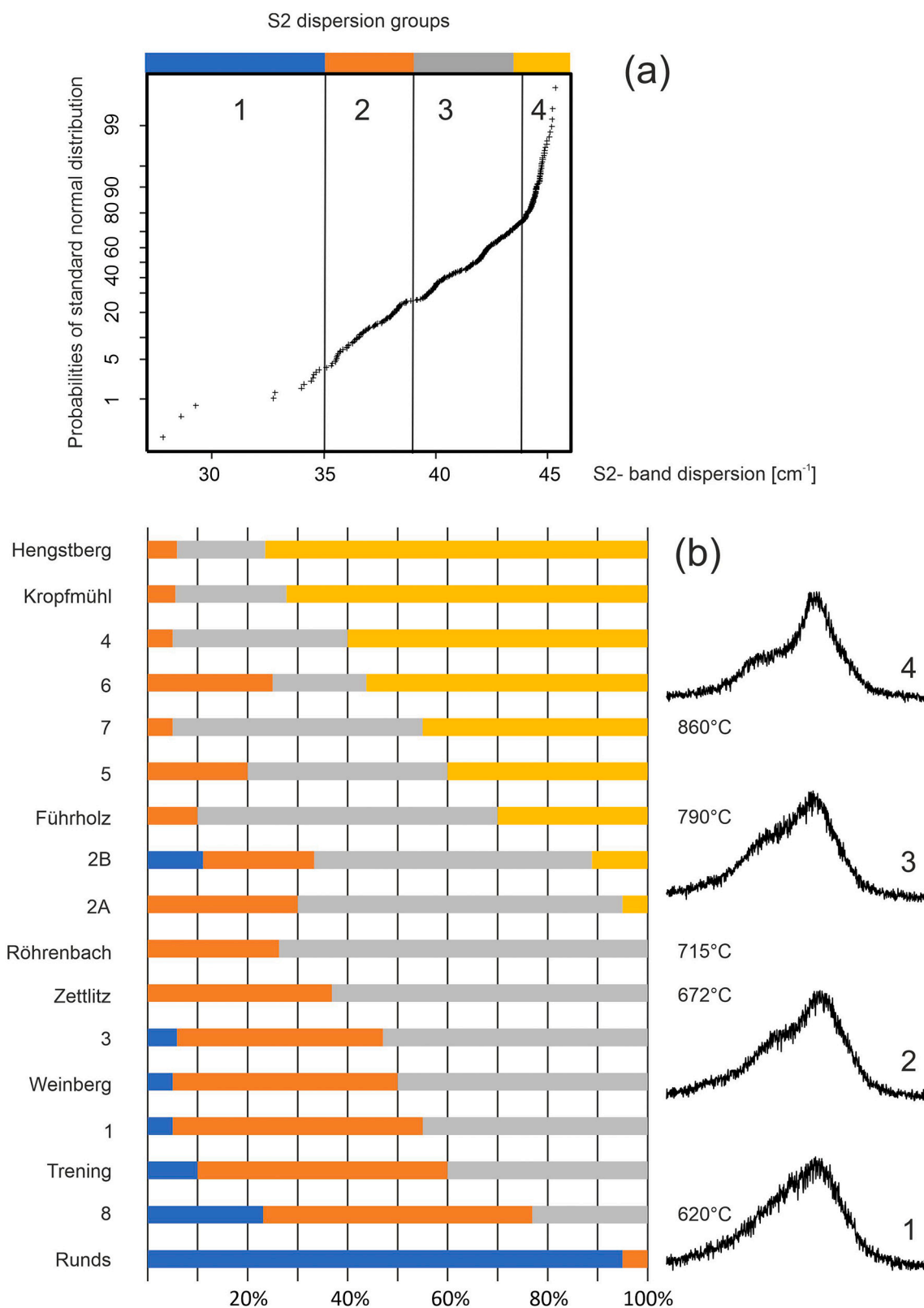
Fig. 5. In a compilation of all sample data ($n = 339$, Table 2), the distances between the two function maxima of the deconvoluted S2-band (S2 dispersion) indicate four graphite types (a). The corresponding sample compositions (b) constrain a trend of increasing distances of the D2 bands with an increase of metamorphic temperatures (bottom to top bars), estimated petrologically from nearby locations (Table 2). The S2-band evolution is illustrated in (b) by spectra from sample 2B.
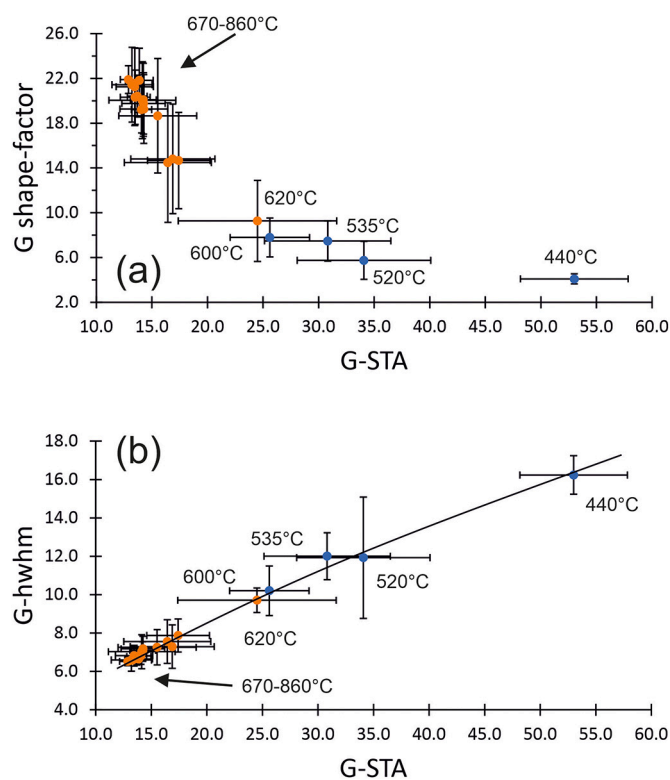
Fig. 6. G- (graphite) shape factor (a) and G- (graphite) band width (G-hwhm) (b) versus G-STA (Lünsdorf et al., 2017) of the Bohemian Massif samples (orange) together with IFORS calibration samples (blue). Error bars indicate the standard deviation. The G-STA parameter predicts metamorphic peak temperatures at temperatures below 600 °C. Temperature estimates from the Bohemian Massif are based on high-grade metamorphic samples with a close proximity to well-constrained calibration samples (samples from the Pleißing Nappe, Zettlitz sample of the Drosendorf Nappe, and Bavarian Massif, Table 2), suggesting a continuation of the trend. (For interpretation of the references to colour in this figure legend, the reader is referred to the web version of this article.)

6. Discussion

The IFORS temperature estimator is calibrated at temperatures higher than 400 °C by the G-STA value (Lünsdorf et al., 2017). This temperature range is identified by a G-shape factor of >3.0. Decreasing G-STA values indicate rising metamorphic temperatures, paralleling a G-band shift to lower wave numbers and a progressive intensity loss of the D2-band, thus, resulting in increasing G-shape factors (Lünsdorf et al., 2017). The graphite data in this study reflect this trend (Fig. 6). As shown in Fig. 6, the observed parameters are also in line with the trends of the IFORS calibration, valid below 600 °C. In the 600 °C reference sample, graphite is present (Rantitsch et al., 2020). According to XRD- and TEM calibration data (Rantitsch et al., 2016a, 2016b), semi-graphite prevails in samples at temperatures lower than 535 °C, suggesting the emergence of full-ordered graphite in the temperature range in-between. In sample 8, crystals smaller than 4 μm with a lattice-ordering in equilibrium to the given metamorphic rank occur together with larger better-ordered graphite crystals. This demonstrates the continuous transitional nature of graphitization at temperatures of 620 °C producing structurally highly variable graphite crystals (see also the error bar of the Pleißing Nappe sample in Fig. 4). In samples of a higher metamorphic rank, the first-order Raman parameter are

distributed unimodally, indicating a more homogeneous crystal composition.

The data in this study demonstrate a major change of the G-band shape (Fig. 6a) between 600 °C and 650 °C. The further modification of the G-band proceeds in a narrower G-STA interval as seen in the 400–600 °C range (Fig. 6a). Here it is important to note the missing break in the G-band width evolution (Fig. 6b) which is seen in the G-band shape versus G-STA correlation (Fig. 6a). Consequently, confirming previous observations (Marques et al., 2009; Kwiecinska et al., 2010; Rodrigues et al., 2013; Kouketsu et al., 2014; Rantitsch et al., 2016a, 2016b; Zhang et al., 2020), this parameter is superior to record the structural evolution of graphite at metamorphic temperatures higher than 600 °C. Furthermore, it is directly related to the lattice dislocation density (Krishna et al., 2017) and represents therefore an intrinsic material property.

Samples from locations of well-constrained P-T conditions demonstrate a correlation between peak metamorphic temperatures and S2 dispersion, G-STA, G-shape factor and G-band width (Figs. 5, 6), thus supporting the conclusions above. A direct use of those parameters as temperature estimators is prevented by a significant uncertainty of any regression results (see Fig. 6). In a regression model, the uncertainty of the calibration data (ca. 30°-50 °C) is obviously multiplied by the uncertainty of the Raman parameters (Table 2). However, if the S2 dispersion parameter is used directly, a map (Fig. 7) shows the spatial variation in the graphite microstructure within the brackets of the calibration dataset (620–860 °C):

The metamorphic peak temperatures in the Drosendorf Nappe and Gföhl Nappe-system and the Pleißing Nappe range between 620 and 785 °C (see above). This broad temperature range is explained partly by an estimator uncertainty of 30–50 °C. However, as seen by reported peak temperatures from the Drosendorf Nappe (Sorger, 2020), a metamorphic field gradient controls a slight northwestern decrease of graphite order to lower structural levels of the Drosendorf Nappe (Fig. 7). The Raman parameters estimate a significant higher lattice ordering in the samples of the Bavarian Massif, calibrated by a temperature estimate of 830–900 °C. The same structure is also observed in two samples from the Gföhl Nappe-system and in the Hengstberg sample of the Drosendorf Nappe. In this sample group, large graphite flakes are observed (Fig. 2a). In map view (Fig. 7), a proximity of higher-grade samples of the Gföhl Nappe-system to the granulite diapir of Sankt Leonhard is obvious. The Hengstberg sample of the Drosendorf Nappe is very close to the granulite diapir of the Dunkelsteinerwald. The extraordinary high degree of graphitization in this sample, suggests a causal relation to granulite exhumation. In accordance to thermometric data of the surroundings (Sorger, 2020), this is not observed in the Zettlitz and Weinberg–Trening areas. The samples from the Bavarian Massif show a well-ordered graphite structure, similar to the Hengstberg sample. Thus, there is evidence that low-pressure and high-temperature metamorphism at temperatures above 830 °C in the Bavarian Massif as well as advective heat transport by rising granulite diapirs in the Gföhl Nappe-system improved the graphite lattice ordering significantly.

7. Conclusions

At the southern margin of the Bohemian Massif, graphite crystals appear in amphibolite- and granulite-facies metamorphic metasediments with peak-metamorphic temperatures higher than 650 °C. Large graphite flakes emerge in rocks affected by more than 800 °C. The latter graphite type is found in the southern Bohemian Massif in areas of low-pressure and high-temperature metamorphism and in localities close to exhumed granulite diapirs. At similar lithostatic pressure conditions, the
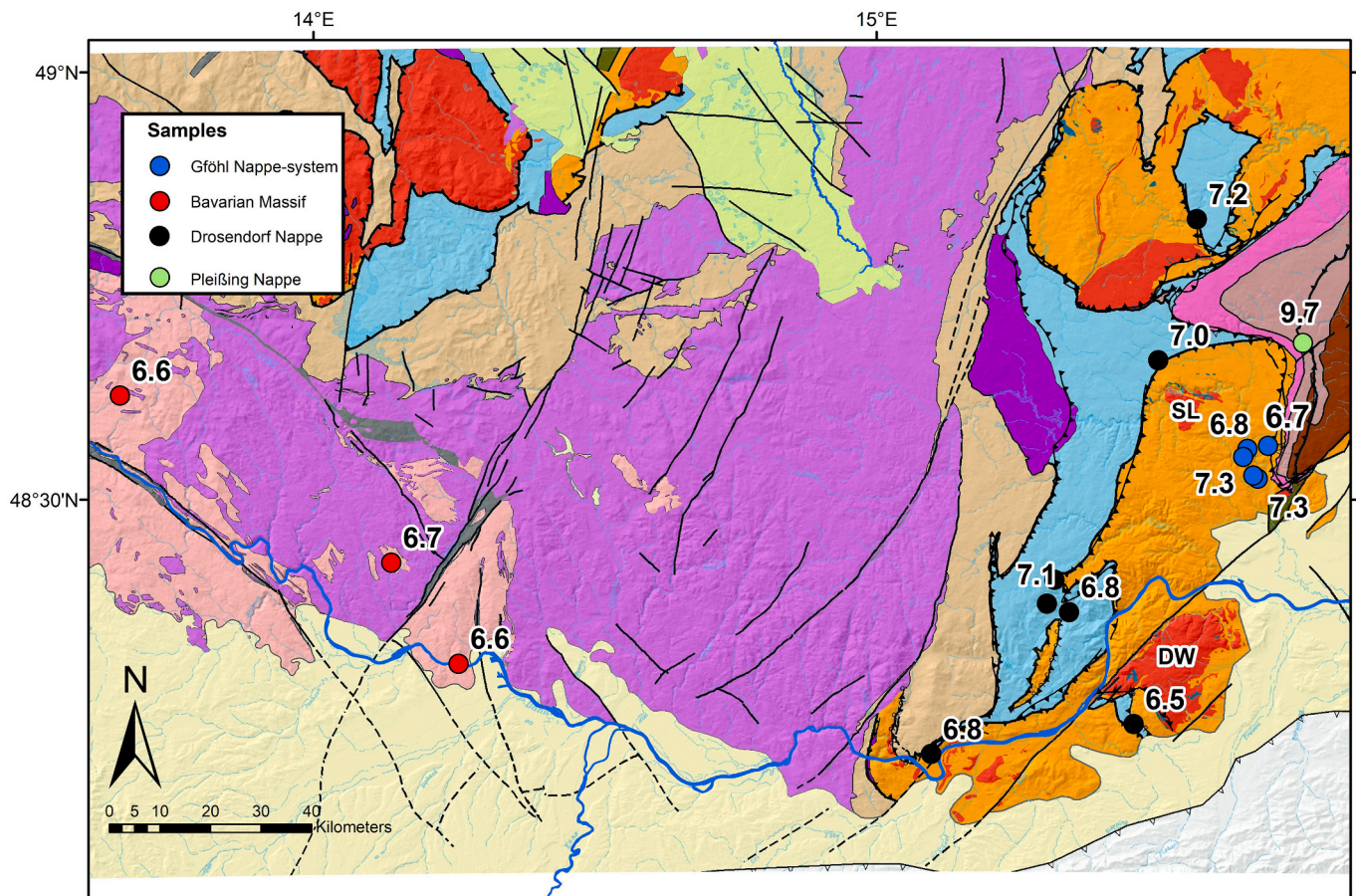
Fig. 7. Half-width at half-maximum of the graphite band (G-hwhm, Table 2) of carbonaceous matter within the southern Bohemian Massif (legend in Fig. 1). Lower values indicate a better structural order and correspondingly higher metamorphic temperatures (DW = granulite diapir of Dunkelsteinerwald, SL = granulite diapir of Sankt Leonhard).

width of the G- (graphite) Raman band as a measure of the lattice dislocation density and the S2-band dispersion as a measure of the stacking order estimate confidently the degree of graphitization, being related to peak metamorphic temperatures. The parameters are useful to map the degree of microstructural order in a medium- to high-grade metamorphic terrain at metamorphic temperatures above 600 °C. Preliminary data suggest that empirical data support a thermometric calibration of Raman spectroscopy data collected on carbonaceous matter which were transformed in high-grade metamorphic terrains.

CRediT authorship contribution statement

Gerd Rantitsch: Conceptualization, Investigation, Formal analysis, Visualization, Writing-original draft, Writing - review & editing . **Manfred Linner:** Investigation, Writing-original draft, Validation, Visualization.

Declaration of Competing Interest

The authors declare that they have no known competing financial interests or personal relationships that could have appeared to influence the work reported in this paper.

References

Beyssac, O., Rouzaud, J.-N., Goffé, B., Brunet, F., Chopin, C., 2002. Graphitization in a high-pressure, low-temperature metamorphic gradient: a Raman microspectroscopy and HRTEM study. Contrib. Mineral. Petrol. 143, 19–31. https://doi.org/10.1007/s00410-001-0324-7.

Bustin, R.M., Rouzaud, J.-N., Ross, J.V., 1995. Natural graphitization of anthracite: Experimental considerations. Carbon 33, 679–691. https://doi.org/10.1016/0008-6223(94)00155-S.

Cançado, L.G., Takai, K., Enoki, T., Endo, M., Kim, Y.A., Mizusaki, H., Speziali, N.L., Jorio, A., Pimenta, M.A., 2008. Measuring the degree of stacking order in graphite by Raman spectroscopy. Carbon 46, 272–275. https://doi.org/10.1016/j.carbon.2007.11.015.

Cháb, J., Breiter, K., Fatka, O., Hladil, J., Kalvoda, J., Šimůnek, Z., Štorch, P., Vašíček, Z., Zajíc, J., Zapletal, J., 2010. Outline of the Geology of the Bohemian Massif. Czech Geological Survey, Prague, pp. 1–294.

Cooke, R., O'Brien, P., 2001. Resolving the relationship between high P–T rocks and gneisses in collisional terranes: an example from the Gföhl gneiss–granulite association in the Moldanubian Zone, Austria. Lithos 58, 33–54. https://doi.org/10.1016/S0024-4937(01)00049-4.

Cui, N., Sun, L., Bagas, L., Xiao, K., Xia, J., 2017. Geological characteristics and analysis of known and undiscovered graphite resources of China. Ore Geol. Rev. 91, 1119–1129. https://doi.org/10.1016/j.oregeorev.2017.09.023.

Dallmeyer, R., Neubauer, F., Höck, V., 1992. Chronology of late Paleozoic tectonothermal activity in the southeastern Bohemian Massif, Austria (Moldanubian and Moravo-Silesian zones): $^{40}Ar/^{39}Ar$ mineral age controls. Tectonophysics 210, 135–153. https://doi.org/10.1016/0040-1951(92)90132-P.

Finger, F., Gerdes, A., Janoušek, V., René, M., Riegler, G., 2007. Resolving the Variscan evolution of the Moldanubian sector of the Bohemian Massif: the significance of the Bavarian and the Moravo-Moldanubian tectonometamorphic phases. J. Geosci. 52, 9–28. https://doi.org/10.3190/jgeosci.005.

Finger, F., Gerdes, A., René, M., Riegler, G., 2009. The Saxo-Danubian Granite Belt: magmatic response to post-collisional delamination of mantle lithosphere below the

southwestern sector of the Bohemian Massif (Variscan orogen). Geol. Carpath. 60, 205–212. https://doi.org/10.2478/v10096-009-0014-3.

Franěk, J., Schulmann, K., Lexa, O., 2006. Kinematic and rheological model of exhumation of high pressure granulites in the Variscan orogenic root: example of the Blanský les granulite, Bohemian Massif, Czech Republic. Mineral. Petrol. 86, 253–276. https://doi.org/10.1007/s00710-005-0114-4.

Friedl, G., Cooke, R.A., Finger, F., McNaughton, N.J., Fletcher, I.R., 2011. Timing of Variscan HP-HT metamorphism in the Moldanubian Zone of the Bohemian Massif: U-Pb SHRIMP dating on multiply zoned zircons from a granulite from the Dunkelsteiner Wald Massif, Lower Austria. Mineral. Petrol. 102, 63–75. https://doi.org/10.1007/s00710-011-0162-x.

Fritz, H., Dallmeyer, R.D., Neubauer, F., 1996. Thick-skinned versus thin-skinned thrusting: Rheology controlled thrust propagation in the Variscan collisional belt (the southeastern Bohemian Massif, Czech Republic - Austria). Tectonics 15, 1389–1413.

Gautneb, H., Rønning, J.S., Engvik, A.K., Henderson, I.H., Larsen, B.E., Solberg, J.K., Ofstad, F., Gellein, J., Elvebakk, H., Davidsen, B., 2020. The graphite occurrences of northern Norway, a review of geology, geophysics, and resources. Minerals 10, 626. https://doi.org/10.3390/min10070626.

Grew, E.S., 1974. Carbonaceous material in some metamorphic rocks of New England and other areas. The Journal of Geology 82, 50–73. https://doi.org/10.1086/627936.

Groß, P., Pleuger, J., Handy, M.R., Germer, M., John, T., 2020. Evolving temperature field in a fossil subduction channel during the transition from subduction to collision (Tauern Window, Eastern Alps). J. Metamorph. Geol. 39, 247–269. https://doi.org/10.1111/jmg.12572.

Henry, D.G., Jarvis, I., Gillmore, G., Stephenson, M., 2019. Raman spectroscopy as a tool to determine the thermal maturity of organic matter: Application to sedimentary, metamorphic and structural geology. Earth Sci. Rev. 102936 https://doi.org/10.1016/j.earscirev.2019.102936.

Iglseder, Ch., Huet, B., Griesmeier, G.E.U., Reiser, M., van Husen, D., 2019. Exkursion 1 (24.06.2019) Grenze Radenthein-Komplex zu Bundschuh-Priedröf-Komplex. Arbeitstagung der Geologischen Bundesanstalt, Wien 2019, Murau, pp. 239–245.

Jamieson, R.A., Beaumont, C., 2013. On the origin of orogens. Geol. Soc. Am. Bull. 125, 1671–1702. https://doi.org/10.1130/B30855.1.

Klötzli, U.S., Frank, W., Scharbert, S., Thöni, M., 1999. Evolution of the SE Bohemian Massif based on geochronological data – a review. Jahrb. Geol. Bundesanst. 141, 377–394.

Kouketsu, Y., Mizukami, T., Mori, H., Endo, S., Aoya, M., Hara, H., Nakamura, D., Wallis, S., 2014. A new approach to develop the Raman carbonaceous material geothermometer for low-grade metamorphism using peak width. Island Arc 23, 33–50. https://doi.org/10.1111/iar.12057.

Kribek, B., Hrabal, J., Landais, P., Hladikova, J., 1994. The association of poorly ordered graphite, coke and bitumens in greenschist facies rocks of the Ponikla Group, Lugicum, Czech Republic: the result of graphitization of various types of carbonaceous matter. J. Metamorph. Geol. 12, 493–503.

Krishna, R., Wade, J., Jones, A.N., Lasithiotakis, M., Mummery, P.M., Marsden, B.J., 2017. An understanding of lattice strain, defects and disorder in nuclear graphite. Carbon 124, 314–333. https://doi.org/10.1016/j.carbon.2017.08.070.

Kwiecińska, B., Petersen, H., 2004. Graphite, semi-graphite, natural coke, and natural char classification—ICCP system. Int. J. Coal Geol. 57, 99–116. https://doi.org/10.1016/j.coal.2003.09.003.

Kwiecinska, B., Suárez-Ruiz, I., Paluszkiewicz, C., Rodriques, S., 2010. Raman spectroscopy of selected carbonaceous samples. Int. J. Coal Geol. 84, 206–212. https://doi.org/10.1016/j.coal.2010.08.010.

Landis, C.A., 1971. Graphitization of dispersed carbonaceous material in metamorphic rocks. Contrib. Mineral. Petrol. 30, 34–45. https://doi.org/10.1007/BF00373366.

Linner, M., 1996. Metamorphism and partial melting of paragneisses of the Monotonous Group, SE Moldanubicum (Austria). Mineral. Petrol. 58, 215–234. https://doi.org/10.1007/BF01172097.

Linner, M., Bayer, I., Schuster, R., Fuchs, G., 2013. Tektonische Gliederung der südlichen Böhmischen Masse abgeleitet aus dem Gesamtdatensatz der Geologischen Bundesanstalt. Arbeitstagung der Geologischen Bundesanstalt 2013, Melk, pp. 106–108.

Lünsdorf, N.K., Lünsdorf, J.O., 2016. Evaluating Raman spectra of carbonaceous matter by automated, iterative curve-fitting. Int. J. Coal Geol. 160–161, 51–62. https://doi.org/10.1016/j.coal.2016.04.008.

Lünsdorf, N.K., Dunkl, I., Schmidt, B.C., Rantitsch, G., von Eynatten, H., 2014. Towards a higher comparability of geothermometric data obtained by Raman spectroscopy of carbonaceous material. Part I: Evaluation of biasing factors. Geostandards and Geoanalytical Research. 38, 73–94. https://doi.org/10.1111/j.1751-908X.2013.12011.x.

Lünsdorf, N.K., Dunkl, I., Schmidt, B.C., Rantitsch, G., von Eynatten, H., 2017. Towards a higher comparability of geothermometric data obtained by Raman spectroscopy of carbonaceous material. Part 2: a revised geothermometer. Geostand. Geoanal. Res. 41, 593–612. https://doi.org/10.1111/ggr.12178.

Lyu, M., Cao, S., Neubauer, F., Li, J., Cheng, X., 2020. Deformation fabrics and strain localization mechanisms in graphitic carbon-bearing rocks from the Ailaoshan-Red River strike-slip fault zone. J. Struct. Geol. 140, 104150. https://doi.org/10.1016/j.jsg.2020.104150.

Marques, M., Suárez-Ruiz, I., Flores, D., Guedes, A., Rodrigues, S., 2009. Correlation between optical, chemical and micro-structural parameters of high-rank coals and graphite. Int. J. Coal Geol. 77, 377–382. https://doi.org/10.1016/j.coal.2008.06.002.

Miranda, D.A., de Oliveira Chaves, A., Campello, M.S., Ramos, S.L.L.D.M., 2019. Origin and thermometry of graphites from Itapecerica supracrustal succession of the

southern Sao Francisco Craton by C isotopes, X-ray diffraction, and Raman spectroscopy. Int. Geol. Rev. 61, 1864–1875. https://doi.org/10.1080/00206814.2018.1564073.

Nakamura, Y., Yoshino, T., Satish-Kumar, M., 2020. Pressure dependence of graphitization: implications for rapid recrystallization of carbonaceous material in a subduction zone. Contrib. Mineral. Petrol. 175, 32. https://doi.org/10.1007/s00410-020-1667-2.

Pasteris, J.D., Wopenka, B., 1991. Raman spectra of graphite as indicators of degree of metamorphism. Can. Mineral. 29, 1–9.

Petrakakis, K., 1997. Evolution of Moldanubian rocks in Austria: review and synthesis. J. Metamorph. Geol. 15, 203–222. https://doi.org/10.1111/j.1525-1314.1997.00015.x.

Petri, B., Štípská, P., Skrzypek, E., Schulmann, K., Corsini, M., Franěk, J., 2014. Thermal and mechanical behaviour of the orogenic middle crust during the syn- to late-orogenic evolution of the Variscan root zone, Bohemian Massif. J. Metamorph. Geol. 32, 599–626. https://doi.org/10.1111/jmg.12081.

Pimenta, M.A., Dresselhaus, G., Dresselhaus, M.S., Cancado, L.G., Jorio, A., Saito, R., 2007. Studying disorder in graphite-based systems by Raman spectroscopy. Phys. Chem. Chem. Phys. 9, 1276–1290. https://doi.org/10.1039/B613962K.

Racek, M., Štípská, P., Pitra, P., Schulmann, K., Lexa, O., 2006. Metamorphic record of burial and exhumation of orogenic lower and middle crust: a new tectonothermal model for the Drosendorf window (Bohemian Massif, Austria). Mineral. Petrol. 86, 221–251. https://doi.org/10.1007/s00710-005-0111-7.

Rantitsch, G., Lämmerer, W., Fisslthaler, E., Mitsche, S., Kaltenböck, H., 2016a. On the discrimination of semi-graphite and graphite by Raman spectroscopy. Int. J. Coal Geol. 159, 48–56. https://doi.org/10.1016/j.coal.2016.04.001.

Rantitsch, G., Lämmerer, W., Fisslthaler, E., Mitsche, S., Kaltenböck, H., 2016b. Erratum to: "On the discrimination of semi-graphite and graphite by Raman spectroscopy". International Journal of Coal Geology 167, 238. https://doi.org/10.1016/j.coal.2016.09.010.

Rantitsch, G., Iglseder, C., Schuster, R., Hollinetz, M.S., Huet, B., Werdenich, M., 2020. Organic metamorphism as a key for reconstructing tectonic processes: a case study from the Austroalpine unit (Eastern Alps). Int. J. Earth Sci. 109, 2235–2253. https://doi.org/10.1007/s00531-020-01897-7.

Rodrigues, S., Marques, M., Suárez-Ruiz, I., Camean, I., Flores, D., Kwiecinska, B., 2013. Microstructural investigations of natural and synthetic graphites and semi-graphites. Int. J. Coal Geol. 111, 67–79. https://doi.org/10.1016/j.coal.2012.06.013.

Schantl, P., Hauzenberger, C., Finger, F., Müller, T., Linner, M., 2019. New evidence for the prograde and retrograde PT-path of high-pressure granulites, Moldanubian Zone, Lower Austria, by Zr-in-rutile thermometry and garnet diffusion modelling. Lithos 342-343, 420–439. https://doi.org/10.1016/j.lithos.2019.05.041.

Schrauder, M., Beran, A., Hoernes, S., Richter, W., 1993. Constraints on the origin and the genesis of graphite-bearing rocks from the variegated sequence of the Bohemian Massif (Austria). Mineral. Petrol. 49, 175–188. https://doi.org/10.1007/BF01164593.

Schulmann, K., Kröner, A., Hegner, E., Wendt, I., Konopásek, J., Lexa, O., Štipska, P., 2005. Chronological constraints on the pre-orogenic history, burial and exhumation of deep-seated rocks along the eastern margin of the Variscan Orogen, Bohemian Massif, Czech Republic. Am. J. Sci. 305, 407–448. https://doi.org/10.2475/ajs.305.5.407.

Skrzypek, E., 2021. First- and second-order Raman spectra of carbonaceous material through successive contact and regional metamorphic events (Ryoke belt, SW Japan). Lithos 388-389, 106029. https://doi.org/10.1016/j.lithos.2021.106029.

Sorger, D., 2020. Metamorphic and Tectonic Evolution of the Drosendorf and Gföhl units – Lower Austria, Bohemian Massif. PhD thesis. University of Graz.

Sorger, D., Hauzenberger, C.A., Linner, M., Iglseder, C., Finger, F., 2018. Carboniferous polymetamorphism recorded in paragneiss-migmatites from the Bavarian Unit (Moldanubian Superunit, Upper Austria): implications for the tectonothermal evolution at the end of the Variscan orogeny. J. Petrol. 59, 1359–1382. https://doi.org/10.1093/petrology/egy063.

Sorger, D., Hauzenberger, C.A., Finger, F., Linner, M., 2020. Two generations of Variscan garnet: Implications from a petrochronological study of a high-grade Avalonia-derived paragneiss from the Drosendorf unit, Bohemian Massif. Gondwana Res. 85, 124–148. https://doi.org/10.1016/j.gr.2020.04.004.

Štípská, P., Hacker, B.R., Racek, M., Holder, R., Kylander-Clark, A.R.C., Schulmann, K., Hasalová, P., 2015. Monazite dating of prograde and retrograde P–T–d paths in the Barrovian terrane of the Thaya window, Bohemian Massif. J. Petrol. 56, 1007–1035. https://doi.org/10.1093/petrology/egv026.

Tropper, P., Deibl, I., Finger, F., Kaindl, R., 2006. P–T–t evolution of spinel–cordierite–garnet gneisses from the Sauwald Zone (Southern Bohemian Massif, Upper Austria): is there evidence for two independent late-Variscan low-P/high-T events in the Moldanubian Unit? Int. J. Earth Sci. 95, 1019–1037. https://doi.org/10.1007/s00531-006-0082-x.

Wojdyr, M., 2010. Fityk: a general-purpose peak fitting program. J. Appl. Crystallogr. 43, 1126–1128. https://doi.org/10.1107/S0021889810030499.

Wopenka, B., Pasteris, J.D., 1993. Structural characterization of kerogens to granulite-facies graphite: applicability of Raman microprobe spectroscopy. Am. Mineral. 78, 533–557.

Wyhlidal, S., Tropper, P., Thöny, W.F., Kaindl, R., 2009. Minor element- and carbonaceous material thermometry of high-grade metapelites from the Sauwald Zone, Southern Bohemian Massif (Upper Austria). Mineral. Petrol. 97, 61–74. https://doi.org/10.1007/s00710-009-0081-2.

Yui, T.-F., Huang, E., Xu, J., 1996. Raman spectrum of carbonaceous material: a possible metamorphic grade indicator for low-grade metamorphic rocks. J. Metamorph. Geol. 14, 115–124. https://doi.org/10.1046/j.1525-1314.1996.05792.x.

Zhang, H.-F., Zhai, M.-G., Santosh, M., Wang, H.-Z., Zhao, L., Ni, Z.-Y., 2014. Paleoproterozoic granulites from the Xinghe graphite mine, North China Craton: Geology, zircon U–Pb geochronology and implications for the timing of deformation, mineralization and metamorphism. Ore Geol. Rev. 63, 478–497. https://doi.org/10.1016/j.oregeorev.2014.03.014.

Zhang, S., Liu, Q., Zhang, H., Ma, R., Li, K., Wu, Y., Teppen, B.J., 2020. Structural order evaluation and structural evolution of coal derived natural graphite during graphitization. Carbon 157, 714–723. https://doi.org/10.1016/j.carbon.2019.10.104.

Zheng, Z., Zhang, J., Huang, J.Y., 1996. Observations of microstructure and reflectivity of coal graphites for two locations in China. Int. J. Coal Geol. 30, 277–284. https://doi.org/10.1016/0166-5162(95)00047-X.